Journal of Power Sources 223 (2013) 277–283

Contents lists available at SciVerse ScienceDirect

Journal of Power Sources

journal homepage: www.elsevier.com/locate/jpowsour

Preparation and properties of cross-linked sulfonated poly(imide-siloxane) for polymer electrolyte fuel cell application

Chao-Chieh Lin, Chuan-Bi Chang, Yen-Zen Wang*

Department of Chemical Engineering and Materials Engineering, National Yunlin University of Science and Technology, 123 University Road, Section 3, Douliou, Yunlin 64002, Taiwan, ROC

HIGHLIGHTS

- The cSPI-SX is obtained by radical polymerization onto the silylmethyl group of PDMS.
- The unique phase separated morphology of cSPI-SX supports the hydrolytic stability.
- The PEFC assembled with cSPI-SX membrane has showed high power output.

ARTICLE INFO

Article history:
Received 14 May 2012
Received in revised form
14 September 2012
Accepted 15 September 2012
Available online 26 September 2012

Keywords:
Sulfonated polyimide
Poly(dimethylsiloxane)
Cross-linked networks
Polymer electrolyte membrane
Fuel cell

ABSTRACT

Cross-linked sulfonated poly(imide-siloxane) (cSPI-SX) is obtained by radical polymerization onto the silylmethyl group of poly(dimethylsiloxane) (PDMS). The chemical structure of the cSPI-SX thus formed is characterized by FT-IR and ^{13}C NMR. The properties required for a proton exchange membrane, such as ion exchange capacity, water uptake, dimensional change, hydrolytic stability, and proton conductivity, are measured and investigated in detail. A transmission electron microscopic (TEM) image shows the presence of large, well-connected hydrophilic domains that are responsible for the high proton conductivity of the cSPI-SX membrane. The unique phase separated morphology of the cSPI-SX membrane supports the outstanding hydrolytic stability. A PEFC assembled with the cSPI-SX membrane has showed high power output at a humidifier gas temperature of 30 °C, a cell operating temperature of 70 °C and a gas pressure of 0.3 MPa.

1. Introduction

As environmental concerns increase, polymer electrolyte fuel cells (PEFCs) have attracted considerable interest as sources of clean energy for transportable, stationary, and portable power applications, because they are highly efficient and cause little environmental pollution [1,2]. A polymer electrolyte is the key component of a PEFC system and it functions as a proton conductor and separates the fuel from the anode and cathode. Perfluorosulfonate ionomers (PFSI), such as DuPont's Nafion membranes, are commercially available and have the advantages of high proton conductivity, excellent chemical stability, and long-term stability. However, they have limited industrial applications due to their high cost, high gas permeability, low operating temperature below 80 °C, and the environmental inadaptability of fluorinated materials [3,4]. Many researchers have sought to develop alternative polymer electrolyte membranes that are based on partially perfluorinated [5–8] and sulfonated hydrocarbon polymers [9–28].

Of various sulfonated polymers, sulfonated polyimide (SPI) with a six-member imide ring is recognized as one of the most promising materials for fuel cell applications due to their excellent properties of high thermal stability, excellent mechanical strength, superior chemical resistance, good film forming ability and very low methanol permeability [9–16]. However, the sulfonic group of SPI has lower acidity than that of perfluorosulfonated polymers [13]. Therefore, SPI must be increased by a high degree of sulfonation to promote its proton conductivity. At high sulfonation levels, most SPI membranes encounter problems that are associated with swelling, and hydrolytic stability. To solve these problems, SPI membranes are modified by chemically modified monomers [29–32], polymer blending [33,34], and cross-linking [35–37]. These have exhibited improved performance and have

* Corresponding author. Tel.: +886 5 534 2601x4617; fax: +886 5 531 2071.
E-mail address: wangzen@yuntech.edu.tw (Y.-Z. Wang).

0378-7753/$ – see front matter © 2012 Elsevier B.V. All rights reserved.
http://dx.doi.org/10.1016/j.jpowsour.2012.09.068

attracted considerable attention. One of the simplest methods for improving hydrolytic stability involves cross-linking.

In our previous work, sulfonated poly(imide-siloxane) (SPI-SX) was synthesized from 1,4,5,8-naphthalenetetracarboxylic dianhydride (NTDA), 4,4′-oxydianiline (ODA), 2,2′-benzidinedisulfonic acid (BDSA), and α,ω-diaminopropyl poly(dimethylsiloxane) (PDMS) [38]. The results show that the appending of highly flexible siloxane segments to the SPI backbone enhances proton conductivity; suppresses swelling, and influences membrane morphology. However, the ion exchange capacity (IEC) must be further increased to improve the proton conductivity of the SPI-SX. In this work, the mole proportion of BDSA in the SPI-SX is increased and radical polymerization is applied to the silylmethyl group of siloxane segments, initiated by benzoyl peroxide (BPO) [39,40]. Introducing a crosslink segment into the SPI-SX membrane not only maintained the degree of sulfonation but also improved the stability of the membrane.

In this work, an SPI-SX membrane was cross-linked by radical polymerization onto the silylmethyl group of poly(dimethylsiloxane). The properties of polymer electrolyte, such as ion exchange capacity, water uptake, dimensional change, hydrolytic stability, and proton conductivity, were investigated in detail. The performance of the SPI membrane, SPI-SX membrane, and cSPI-SX in a polymer electrolyte fuel fell (PEFC) was compared to that of Nafion 212 membrane.

2. Experimental

2.1. Materials

The 1,4,5,8-naphthalenetetracarboxylic dianhydride (NTDA, 95% pure; Aldrich) was dried under vacuum before use. The 4,4′-oxydianiline (ODA, 98% pure; Aldrich) was used without further purification. The 2,2′-benzidinedisulfonic acid (BDSA, 70% pure; Tokyo Chemical Industry Co.) was dissolved in ethanol and was neutralized with triethylamine (TEA, 99.9% pure; Sigma–Aldrich) at 60 °C. The BDSA-TEA was purified by recrystallization from the ethanol solution and was dried under vacuum for 3 days. The α,ω-diaminopropyl poly(dimethylsiloxane) (PDMS) (Shin-Etsu Chemical; $M_w = 850$ g mol^{-1}) was used without further purification. Benzoic acid (BA, 99.5% pure; Sigma–Aldrich) and benzoyl peroxide (BPO, 75%; Sigma–Aldrich) were used without further purification. *m*-Cresol (99% pure; Sigma–Aldrich) and Nafion-containing solution (Nafion® PFSA polymer dispersion, 5 wt%; DuPont Fuel Cells) were used without further purification.

2.2. Preparation of sulfonated polyimide membranes

Sulfonated polyimide (SPI) was prepared from NTDA, BDSA-TEA and ODA according to a method that has been described elsewhere [41], with an NTDA:BDSA-TEA:ODA molar ratio of 0.93:0.64:0.29. A randomly sulfonated poly(imide-siloxane) (SPI-SX) copolymer was prepared from NTDA, BDSA-TEA, ODA, and α,ω-diaminopropyl poly(dimethylsiloxane) (PDMS) according to a method that has been described elsewhere [38], with an NTDA:BDSA-TEA:ODA:PDMS molar ratio of 0.93:0.64:0.25:0.04. The SPI membrane and SPI-SX membrane were prepared by casting with 5 wt% *m*-cresol solutions (in TEA form) onto glass plates followed by drying in an oven at 80 °C for 12 h to remove residual solvent. The SPI-SX (TEA salt form) was dissolved in *m*-cresol, which was then stirred with BPO in an N_2 atmosphere at 30 °C for 12 h. The PDMS:BPO molar ratio was 1:3. The solution was cast onto a glass plate and dried in an oven at 80 °C for 12 h to remove residual solvent and at 130 °C for 12 h to initiate the radical polymerization onto the silylmethyl group of PDMS [39]. The prepared membranes, roughly 50 ± 10 μm thick, were soaked in 1 M H_2SO_4 at room temperature for 24 h to transform the TEA salt into protonated form. These membranes were then thoroughly washed with de-ionized (DI) water. Scheme 1 shows the chemical structures of SPI-SX and cross-linked SPI-SX.

2.3. Polymer characterization

The prepared membranes were examined by Fourier transform infrared (FT-IR) spectroscopy with attenuated total reflection (ATR) (Spectrum One, Perkin Elmer). Signal-averaging was performed over a minimum of 8 scans with a resolution of 2 cm^{-1} in the 4000–650 cm^{-1} range. ^{13}C NMR spectra were recorded on solid state NMR (Avance 400, Bruker). Thermogravimetric analysis (TGA) (Q500, TA Instruments) was performed to estimate the thermal stability of membranes and the water weight loss of the hydrated membranes. The temperature was increased to 900 °C at a rate of 10 °C min^{-1} in a nitrogen atmosphere. The weight of the sample was about 7 ± 2 mg.

2.4. Ion exchange capacity

The ion exchange capacity was measured using the titration method. Dried membranes were crushed using a cryogenic crusher and then soaked in 1 M NaCl solution for 48 h to release protons. Released protons were titrated using 0.01 M NaOH solution, using phenolphthalein indicator. The IEC value was recorded as an average value of each sample in milliequivalent NaOH per gram polymer (meq g^{-1}).

2.5. Water uptake and dimensional change

Water absorption of the membranes was determined at 30 °C. These membranes were dried in a vacuum at 100 °C for 24 h, weighed, and then immersed in de-ionized (DI) water at room temperature for 24 h. Wet membranes were dried by wiping and then weighed immediately. Water uptake (WU) of membranes was obtained from weight percentage, using the following equation:

$$\mathrm{WU}\ (\%) = \frac{W_{\mathrm{wet}} - W_{\mathrm{dry}}}{W_{\mathrm{dry}}} \times 100\%$$

Dimensional changes were derived as follows:

$$\Delta l_c = \frac{l_w - l_d}{l_d} \times 100\%$$

$$\Delta t_c = \frac{t_w - t_d}{t_d} \times 100\%$$

where t_d and l_d are the thickness and the length, respectively, of a membrane that is dried in a vacuum at 100 °C for 24 h, and t_w and l_w are the thickness and length of a membrane that is immersed in DI water at room temperature for 24 h.

2.6. Proton conductivity

Transverse proton conductivities of membranes were measured using an AC impedance analyzer (PGSTA30, Autolabe) over a frequency range of 1–10,000 kHz. The hydrated membranes were sandwiched between two stainless steel electrodes, and placed in a temperature-controlled cell. The cell was sealed with water over the duration testing [26,28]. Conductivity, σ, in the transverse direction was calculated from impedance data using the following equation:

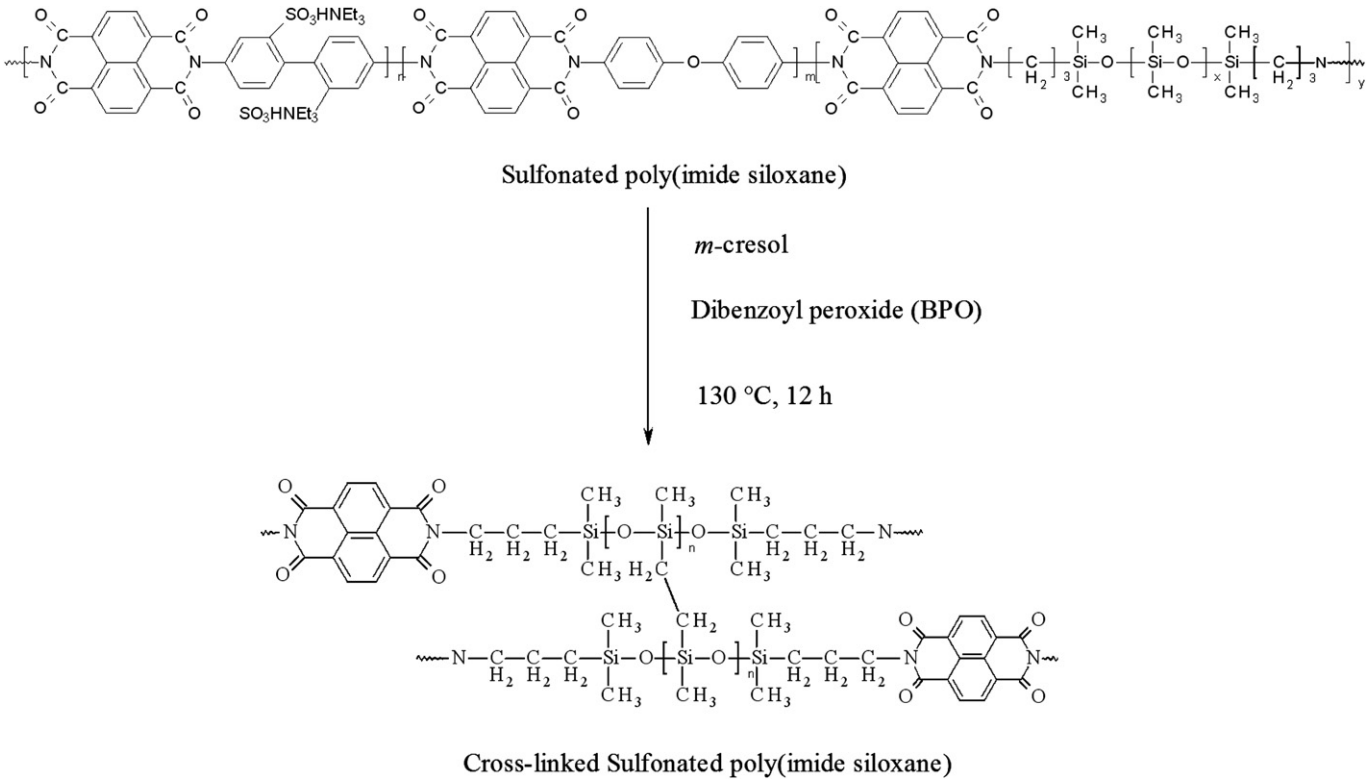

Scheme 1. Synthesis of cSPI-SX.

$$\sigma = \frac{d}{RA}$$

where d and A are the thickness and surface area of a membrane sample, respectively, and R is resistance.

2.7. Hydrolytic stability and oxidative stability

Hydrolytic stability was determined by immersing the membranes into DI water at 80 °C. Stability was assessed as the time required for samples starts to lose their mechanical strength [11].

A small piece of membrane sample (0.5 × 1.0 cm^2) was soaked at 30 °C in Fenton's reagent which is prepared with 30 ppm $FeSO_4$ in 30% H_2O_2. Stability was evaluated by recording the time needed when membranes became a little brittle (time1 = τ_1) and completely dissolved in the reagent (time2 = τ_2) [11].

2.8. Analysis of microstructure

Transmission electron microscopic (TEM) images were recorded using a JOEL TEM-200CX instrument that was operated at 120 kV. The membrane in protonated form was transformed to the $-SO_3Ag$ form by immersing in 0.5 M $AgNO_3$ for 12 h to stain the ionic domains. The dried samples were encapsulated in epoxy resin and cross-sectioned in a microtome to yield the 80 nm thick sections [42–44]. Darker areas in the micrographs were associated with Ag containing, hydrophilic domains.

2.9. Preparation and evaluation of membrane electrode assembly

To fabricate a membrane electrode assembly (MEA) for PEMFC, a 5 wt% Nafion solution (136.2 mg) and a 20 wt% Pt/C (E-TEK) (12.6 mg) were mixed with isopropyl alcohol in a beaker. The Pt/C catalyst loading on the anode and cathode was 0.5 mg Pt per cm^2. An MEA was prepared by hot-pressing the electrode/membrane/electrode into a sandwich at 140 °C for 5 min under 50 $kgfcm^{-2}$. The MEA was put in a single-cell test equipment (active area, 5 cm^2) (Asia Pacific Fuel Cell Technologies, Ltd.), and then was installed in a fuel cell test station (model FCED-P50; Asia Pacific Fuel Cell Technologies, Ltd.). The PEFC performance was evaluated at cell temperatures of 30–70 °C and different gas humidification temperatures of 30–70 °C. The feed rate of H_2 and O_2 was 100 and 200 mL min^{-1}, respectively, with a bulk gas pressure of 0.3 MPa.

3. Results and discussion

3.1. Characterization of membranes

The chemical structure of cross-linked SPI-SX (cSPI-SX) was confirmed by FT-IR and ^{13}C NMR spectrum, respectively. Fig. 1 shows the FT-IR spectra of both SPI-SX and cSPI-SX. The characteristic absorption bands of imide carbonyl groups at 1710 cm^{-1} (asymmetric stretching) and 1670 cm^{-1} (symmetric stretching) reveal the formation of polyimide, and the band at 1345 cm^{-1} was assigned to C–N vibration in the imide ring [45]. No characteristic absorption of polyamic acid was found at around 1780 cm^{-1}, indicating complete imidization [45]. The characteristic absorption bands at 1026 cm^{-1} and 1190 cm^{-1} correspond to the O=S=O symmetric and asymmetric stretching vibrations of aromatic sulfonic acid groups, respectively [11]. The characteristic absorption bands at 2951 cm^{-1} and 881 cm^{-1} were assigned to C–H and Si–C stretching in the siloxane segment. The characteristic absorption bands at 1025–1096 cm^{-1} were assigned to Si–O–Si and Si–O stretching in the siloxane segment. However, this signal was much weaker due to the overlapping with the sulfonic acid groups in the same region [42]. Moreover, the small-scale variation in the peak intensity between CH_3 and CH_2 made it difficult to discern

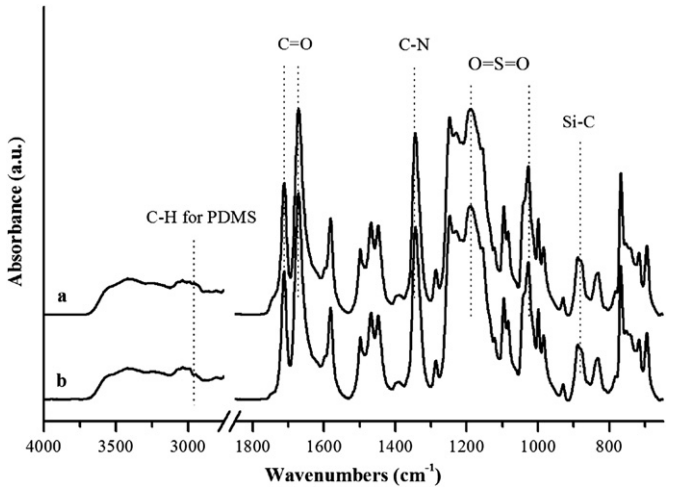

Fig. 1. FT-IR spectrum of the SPI-SX and cSPI-SX membranes.

whether the PDMS is cross-linked or not. Fig. 2 shows the ^{13}C NMR spectra of SPI-SX and cSPI-SX. The peaks at δ 110–166 ppm are assigned to the carbon atoms of SPI [46]. The peaks at δ 30 and 40 ppm are assigned to those of PDMS [47]. The presence of the silylmethylene group of PDMS at 15 ppm showed that the cross-linking did occur on the silylmethyl group of PDMS, as indicated in Scheme 1 [48], in which the entire chemical structure of the cSPI-SX is demonstrated.

3.2. Morphological analysis

Nanoscopic phase separation can occur in a polymer electrolyte membrane because of the coexistence of hydrophobic and hydrophilic segments, which can influence such properties proton conductivity and water uptake. Fig. 3(a)–(d) shows TEM analyses of SPI, SPI-SX, cSPI-SX, and Nafion 212 membranes, respectively. The darker regions represent localized hydrophilic ionic (sulfonate groups) clusters that contain protons, which were stained following the ion exchange with silver ions, while the lighter parts were

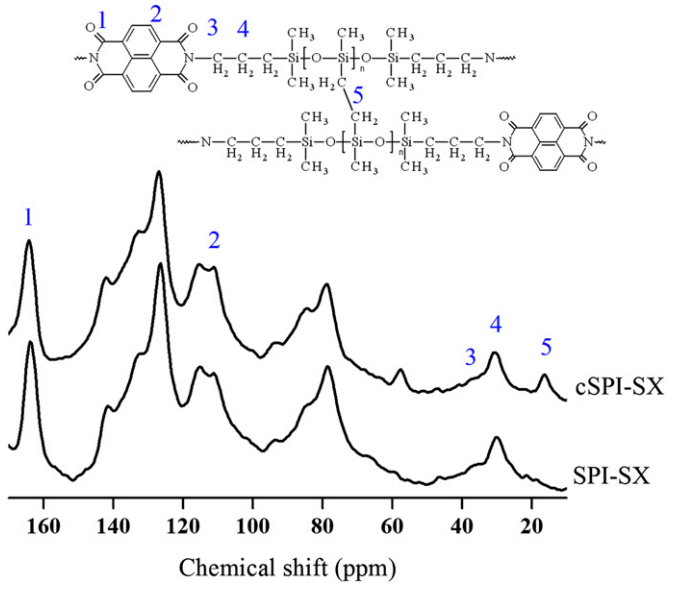

Fig. 2. ^{13}C NMR spectrum of the SPI-SX and cSPI-SX membranes.

hydrophobic regions. Similar morphologies have been observed for other SPIs [43,44]. Huang et al. confirmed the morphological features by using EDX spectrum. The darker regions in the TEM image were silver ions firmly associated with sulfonic group to demonstrate both Ag and S atoms in the EDX spectrum [43]. The numbers of hydrophilic ionic (sulfonate groups) clusters in the SPI, SPI-SX, and cSPI-SX membranes were higher than that in the Nafion 212 membrane, because the SPI series of membranes had high IEC (Table 1). Estimated by the statistics, the sizes of the domains in Fig. 3(a) were between 15 and 20 nm and those in Fig. 3(b) were between 5 and 10 nm. The sizes of the domains in Fig. 3(c) were mostly in the range 30 and 40 nm. The presence of more flexible siloxane segments increased the mobility of the SPI-SX backbone and favored rearrangements that gave rise smaller clusters and enhanced the separation of hydrophobic and hydrophilic phases. However, the hydrophilic ionic clusters in the cSPI-SX membrane had undergone a significant change, and became continuous, forming large channels in the ionic rich phases. This phenomenon was caused by the enhancement of the separation between the hydrophobic and hydrophilic phases by cross-linking silylmethyl group of PDMS.

Therefore, the darker regions found in the TEM image hint the presence of the sulfonic counter ions and the larger hydrophilic clusters in the image are the aggregated sulfonic acid groups which could enlarge the proton transport pathways and significantly improve the proton conductivity.

3.3. Thermal properties

The TGA thermograms were obtained at 40–900 °C with a heating rate of 10 °C min^{-1} in a nitrogen atmosphere. Fig. 4 shows TGA results for fully hydrated SPI, SPI-SX, and cSPI-SX membranes. The figure also shows the derivative thermogravimetric thermograms (DTG). Those of the SPI series of membranes revealed three main weight-loss regions, which appeared as three peaks in the DTG curves. The first region, below 200 °C, was associated with the evaporation of absorbed water from the membranes [49]. The second transition region, which started at 300 °C, was associated with the decomposition of sulfonic acid groups. The third region at around 550 °C, was associated with the cleavage of the backbone of the SPI in the membrane [50]. The SPI series of membranes demonstrated superior thermal properties and can be utilized as polymer electrolyte membranes at high temperatures.

3.4. Properties of polymer electrolyte membranes

Most of the important properties of the polymer electrolyte membranes, such as proton conductivity and water uptake, depend on their IEC, which can be related to the amount of ion exchange sites available for carrying protons. In this work, the IEC values of the SPI-SX and cSPI-SX membranes were lower than that of the SPI membrane (Table 1) because the introduction of PDMS (M_w = 850 g mol^{-1}) increased the equivalent weight and reduced the IEC value. The IEC value of cSPI-SX was lower than that of SPI-SX because the cross-linked structure reduced the rate of release of protons.

Generally, water uptake increases as IEC. In this work, the SPI-SX and cSPI-SX membranes exhibited larger water uptake than the SPI membrane. As described in the TGA experiment (Fig. 4), the weight-loss in the first weight-loss region was greater for the SPI-SX and cSPI-SX membranes than for the SPI membrane, because the presence of the PDMS segments in the SPI-SX structure reduced the 'crowdedness' in the polymer, disfavoring molecular packing [43]. Consequently, the amount of water molecules that were absorbed in the SPI-SX and cSPI-SX membranes increased when

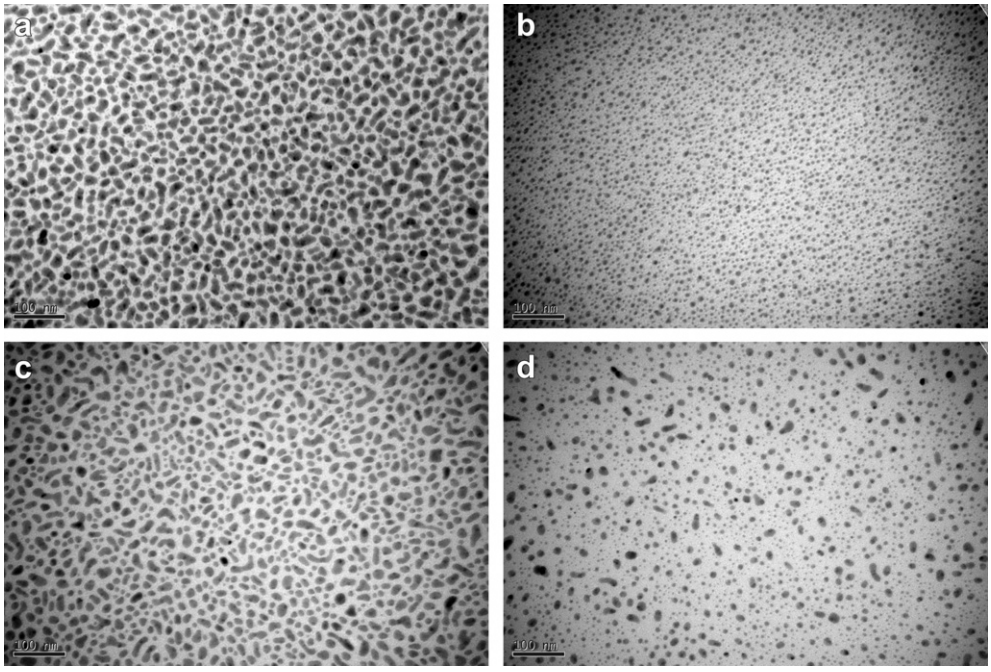

Fig. 3. TEM micrographs of membranes: (a) SPI, (b) SPI-SX, (c) cSPI-SX, and (d) Nafion 212.

PDMS was introduced. Compared to the SPI and SPI-SX membranes, the cSPI-SX membrane exhibited the largest water uptake in this study because the cross-linking of the silylmethyl group of PDMS enhances the phase separation between the hydrophobic and hydrophilic domains, forming large channels in the ionic rich phases (Fig. 3(c)).

As shown in Table 1, the SPI-SX and cSPI-SX membranes exhibited anisotropic membrane swelling. The dimensional change in the transverse direction was larger than that in the plane. This anisotropy was comparable to that of the SPI.

The hydrolytic stability of the SPI series of membranes is a very important factor related to membrane performance. As shown in Table 1, the hydrolytic stability of the cSPI-SX membrane exhibited outstanding and better than that of the SPI membrane. The unique phase separated morphologies of the cSPI-SX membrane support the phenomenon.

Oxidative stability of the membranes was characterized by the elapsed time that the membranes started to become a little brittle (the membranes were broken when lightly bent) or completely dissolved in the reagent. As shown in Table 1, the cSPI-SX membrane exhibited more oxidative stability than that of the SPI-SX membrane. It is attributed to its cross-linked structure.

The Arrhenius plot of proton conductivity of the polymer electrolyte membranes was determined as a function of temperature (Fig. 5). The proton conductivity of the SPI series of membranes and the Nafion 212 membrane increased with temperature because of the dynamics of proton transfer. Moreover, proton transport in membranes requires well connected channels that are formed by ionic clusters of hydrophilic sulfonic acid groups. The size and distribution of these clusters have a decisive effect on the selective transport of protons through the membranes. The SPI-SX membrane exhibited higher proton conductivity than the SPI membrane throughout whole temperature range. The smaller, more dispersed clusters of the SPI-SX membrane are attributed to the incompatibility between the PDMS segments and the ionic-containing polyimides (Fig. 3(b)). The smaller clusters are tightly packed, possibly enabling ionic pathways to form, promoting proton transport [42]. The cSPI-SX membrane exhibited the highest proton conductivity throughout whole temperature range, signifying that larger ionic clusters could accommodate higher contents of water and thereby favorably enhanced the conductivity (Fig. 3(c)).

The mechanism of proton conduction can be understood by examining the activation energy of the process. The Grotthus mechanism is the jumping of the proton to the neighboring lone pair of electrons in the water molecule, and yields an activation energy for proton conduction of between 14 kJ mol^{-1} and 40 kJ mol^{-1}; the vehicle mechanism is the diffusion of the proton in the form of

Table 1
Ion exchange capacity, water uptake, dimensional change, hydrolytic stability, oxidative stability and activation energy of polymer electrolyte membranes.

Membrane	IEC[a] (meq g^{-1})	Water uptake (%)	Dimensional change		Hydrolytic stability[b] (h)	Oxidative stability[c]		Activation energy[d] (kJ mol^{-1})
			Δt_d (%)	Δl_d (%)		τ_1 (h)	τ_2 (h)	
SPI	1.88 ± 0.02	35	25.0	7.2	8	–	–	12.3
SPI-SX	1.85 ± 0.02	40	33.3	6.3	12	32	46	29.9
cSPI-SX	1.82 ± 0.02	47	42.9	6.5	18	45	65	27.1
Nafion 212	0.91 ± 0.01	23	20.0	2.5	–	–	–	4.9

[a] Determined from potentiometric titration.
[b] Determined by immersing membranes into de-ionized water at 80 °C.
[c] τ_1 and τ_2 refer to the elapsed time that the membranes became a little brittle and completely dissolved in the reagent, respectively.
[d] The activation energy derived from the proton conductivity measurement in the temperature range of 30–90 °C at 100% relative humidity.

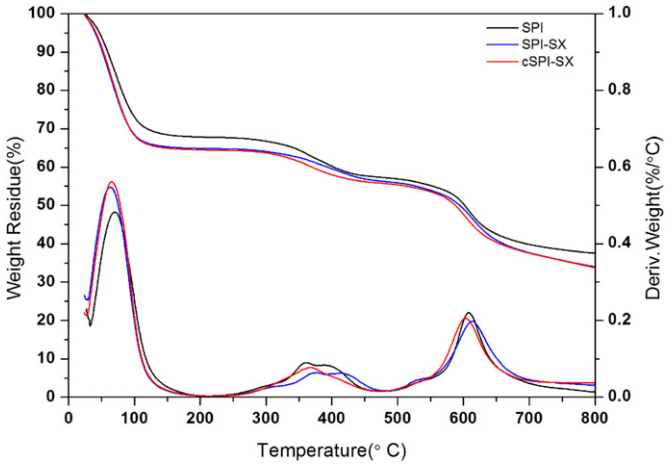

Fig. 4. TGA thermograms of the SPI, SPI-SX, and cSPI-SX membranes.

hydronium ions, such as H_3O^+, or $H_5O_2^+$, in the membrane [51]. Table 1 lists the activation energy of each polymer electrolyte membrane. The SPI series of membranes show more activation energy than the Nafion 212 membrane, indicating that the increase in conductivity with temperature is greater for the SPI series of membranes [43]. Therefore, proton conduction in the SPI-SX and cSPI-SX membranes is described by the Grotthus mechanism.

3.5. PEFC performance

Fig. 6 shows the PEFC performances for the SPI, SPI-SX, cSPI-SX and Nafion 212 at a cell temperature of 30 °C with a feed gas pressure of 0.3 MPa and anode and cathode gas humidification temperatures of 30 °C. Table 2 lists the PEFC performance data in terms of open circuit voltage (OCV), cell voltage at 1.0 A cm^{-2} ($V_{1.0}$), maximum output (W_{max}) and electrode reaction resistance (R_{el}).

At gas humidification temperature of 30 °C, the PEFC performance was in the order of cSPI-SX > Nafion 212 > SPI > SPI-SX. The variation in PEFC performance among SPI, SPI-SX and cSPI-SX seemed to have been caused by the variation in the effect on the back diffusion of water molecules that were formed at the cathode. This was because the large ionic clusters of the cSPI-SX membrane provided more complete proton conduction pathway at gas

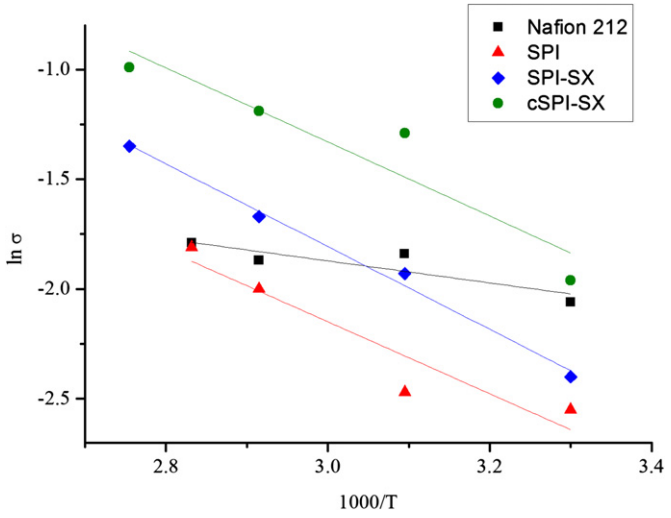

Fig. 5. Proton conductivity of the SPI, SPI-SX, cSPI-SX, and Nafion 212 membranes as a function of temperature.

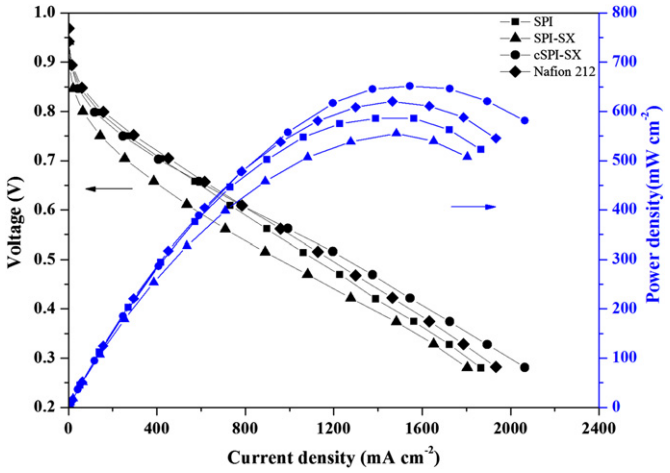

Fig. 6. PEFC performances for SPI, SPI-SX, cSPI-SX and Nafion 212 membranes at cell temperature of 30 °C and gas humidification temperature at 30 °C.

humidification temperature of 30 °C. The polarization curve of the SPI-SX membrane had a larger voltage drop than that of other membranes up to 1.0 A cm^{-2}, indicating that the SPI-SX membrane had higher activation and ohmic loss.

Fig. 7(a) and (b) shows the PEFC performance at 70 °C, 0.3 MPa and anode/cathode gas humidification temperatures of 30 °C and 70 °C, respectively. Increased temperature improved reaction kinetics and membrane conductivity. At gas humidification temperature of 70 °C, the SPI series of membranes exhibited a high PEFC performance, for example, OCV of 0.94–0.95 V, $V_{1.0}$ of 0.58–0.60 V, and maximum output (W_{max}) of 740–764 mW cm^{-2}, which were similar to those of the Nafion 212 membrane. With decreasing humidification of gases, the cell performance largely decreased. This was because the amount of water that could evaporate and go out of the cell with the exhaust gases. However, even under a low humidification at 30 °C, the PEFC performance of the cSPI-SX membrane was still kept at the fairly high level; 0.92 V (OCV), 0.51 V ($V_{1.0}$), 0.0236 Ω (R_{el}), and 619 mW cm^{-2} (W_{max}). These results indicate that the cSPI-SX membrane retained the water content. By combining the microscopic observation and proton conducting behavior, it is concluded that large and well-connected ionic clusters are likely to improve proton transport properties and PEFC performance in the cSPI-SX membranes. Additional studies of the long-term stability and efforts to improve cell performance are currently in progress.

Table 2
PEFC performance data of OCV, cell voltage at 1 A cm^{-2}, maximum output (W_{max}) and electrode reaction resistance (R_{el}) under PEFC operation.

Conditions[a]	Membrane	OCV (V)	$V_{1.0}$ (V)	R_{el}[b] (Ω)	W_{max} (mW cm^{-2})
30/30/0.3	SPI	0.94	0.54	0.0225	592
	SPI-SX	0.94	0.48	0.0318	555
	cSPI-SX	0.94	0.56	0.0235	651
	Nafion 212	0.95	0.54	0.0219	620
30/70/0.3	SPI	0.88	–	0.9828	26
	SPI-SX	0.88	–	0.0814	196
	cSPI-SX	0.92	0.51	0.0236	619
	Nafion 212	0.91	0.29	0.1356	297
70/70/0.3	SPI	0.95	0.6	0.0179	740
	SPI-SX	0.94	0.58	0.0264	764
	cSPI-SX	0.94	0.58	0.0205	745
	Nafion 212	0.97	0.62	0.018	768

[a] PEFC operation conditions: *x*/*y*/*z* refer to gas humidification temperature (°C), cell temperature (°C) and gas pressure (MPa).
[b] Measured at 0.6 V.

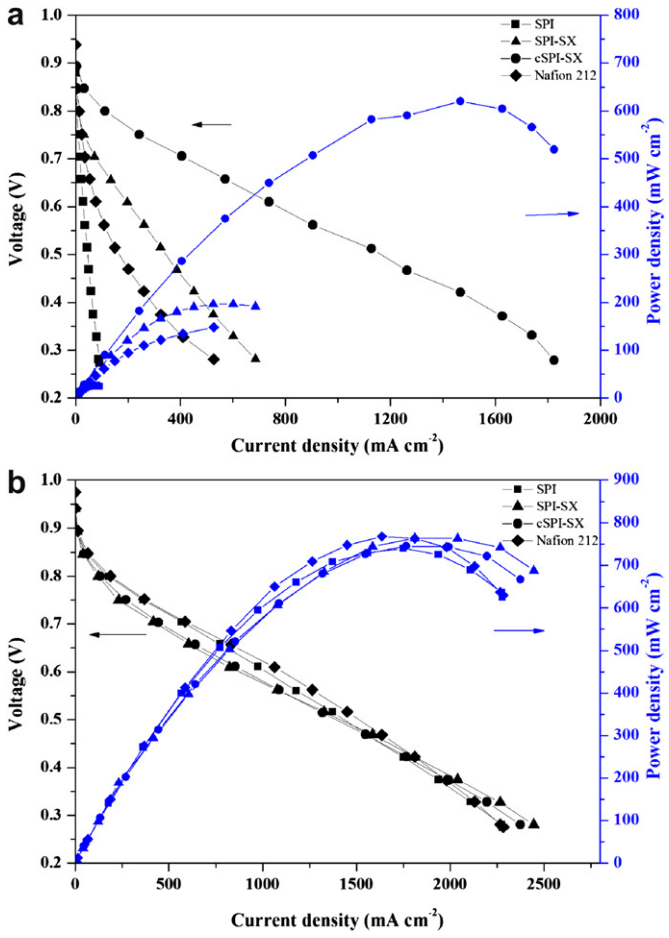

Fig. 7. PEFC performances for SPI, SPI-SX, cSPI-SX and Nafion 212 membranes at cell temperature of 70 °C and gas humidification temperature (a) at 30 °C, (b) at 70 °C.

4. Conclusions

Cross-linked sulfonated poly(imide-siloxane) was synthesized and characterized by the FT-IR and ^{13}C NMR. The introduction of flexible siloxane segments improved the proton conductivity and water uptake. As temperature increased, the proton conductivity of the cross-linked SPI-SX membrane increased more rapidly than that of Nafion 212. Due to the presence of the large and well-connected ionic clusters and flexible siloxane segments, more water can be accommodated within the membrane. The highest PEFC performance 619 mW cm^{-2} was obtained for cross-linked SPI-SX membrane at 70 °C with a relatively low humidification temperature, compared to that of Nafion 212 (297 mW cm^{-2}). The cross-linked SPI-SX membrane can be useful as a high temperature PEMs due to the promoted effect of the back-diffusion water.

Acknowledgment

We gratefully acknowledge the National Science Council, Taipei, Taiwan, for their generous financial support of this research under Contract No. NSC-100-2221-E-224-074.

References

[1] L. Carrette, K.A. Friedrich, U. Stimming, Fuel Cells 1 (2001) 5–39.
[2] B.C.H. Steele, A. Heinzel, Nature 414 (2001) 345–352.
[3] A. Heinzel, V.M. Barragán, Journal of Power Sources 84 (1999) 70–74.
[4] M.A. Hickner, H. Ghassemi, Y.S. Kim, B.R. Einsla, J.E. McGrath, Chemical Reviews 104 (2004) 4587–4612.
[5] C. Yoonoo, C.P. Dawson, E.P.L. Roberts, S.M. Holmes, Journal of Membrane Science 369 (2011) 367–374.
[6] S. Mollá, V. Compañ, Journal of Membrane Science 372 (2011) 191–200.
[7] H. Zhang, H. Huang, P.K. Shen, International Journal of Hydrogen Energy 37 (2012) 6875–6879.
[8] B.G. Choi, J. Hong, Y.C. Park, D.H. Jung, W.H. Hong, P.T. Hammond, H. Park, ACS Nano 5 (2011) 5167–5174.
[9] C. Genies, R. Mercier, B. Sillion, N. Cornet, G. Gebel, M. Pineri, Polymer 42 (2001) 359–373.
[10] S. Besse, P. Capron, O. Diat, G. Gebel, F. Jousse, D. Marsacq, M. Pineri, C. Marestin, R. Mercier, Journal of New Materials for Electrochemical Systems 5 (2002) 109–112.
[11] X. Guo, J. Fang, T. Watari, K. Tanaka, H. Kita, K.-i. Okamoto, Macromolecules 35 (2002) 6707–6713.
[12] K.-i. Okamoto, Y. Yin, O. Yamada, M.N. Islam, T. Honda, T. Mishima, Y. Suto, K. Tanaka, H. Kita, Journal of Membrane Science 258 (2005) 115–122.
[13] B.R. Einsla, Y.S. Kim, M.A. Hickner, Y.-T. Hong, M.L. Hill, B.S. Pivovar, J.E. McGrath, Journal of Membrane Science 255 (2005) 141–148.
[14] Z. Hu, T. Ogou, M. Yoshino, O. Yamada, H. Kita, K.-I. Okamoto, Journal of Power Sources 194 (2009) 674–682.
[15] K.-i. Okamoto, K. Yaguchi, H. Yamamoto, K. Chen, N. Endo, M. Higa, H. Kita, Journal of Power Sources 195 (2010) 5856–5861.
[16] Y. Yin, Q. Du, Y. Qin, Y. Zhou, K.-i. Okamoto, Journal of Membrane Science 367 (2011) 211–219.
[17] L.E. Karlsson, P. Jannasch, Journal of Membrane Science 230 (2004) 61–70.
[18] Z. Li, J. Ding, G.P. Robertson, M.D. Guiver, Macromolecules 39 (2006) 6990–6996.
[19] L. Li, J. Zhang, Y. Wang, Journal of Membrane Science 226 (2003) 159–167.
[20] P. Xing, G.P. Robertson, M.D. Guiver, S.D. Mikhailenko, K. Wang, S. Kaliaguine, Journal of Membrane Science 229 (2004) 95–106.
[21] Q. Guo, P.N. Pintauro, H. Tang, S. O'Connor, Journal of Membrane Science 154 (1999) 175–181.
[22] M.A. Hofmann, C.M. Ambler, A.E. Maher, E. Chalkova, X.Y. Zhou, S.N. Lvov, H.R. Allcock, Macromolecules 35 (2002) 6490–6493.
[23] J. Rhim, H. Park, C. Lee, J. Jun, D. Kim, Y. Lee, Journal of Membrane Science 238 (2004) 143–151.
[24] N. Deluca, Y. Elabd, Journal of Power Sources 163 (2006) 386–391.
[25] T. Yang, International Journal of Hydrogen Energy 33 (2008) 6772–6779.
[26] Y. Huang, L. Chuang, A. Kannan, C. Lin, Journal of Power Sources 186 (2009) 22–28.
[27] C.-Y. Tseng, Y.-S. Ye, K.-Y. Kao, J. Joseph, W.-C. Shen, J. Rick, B.-J. Hwang, International Journal of Hydrogen Energy 36 (2011) 11936–11945.
[28] B.-J. Hwang, J. Joseph, Y.-Z. Zeng, C.-W. Lin, M.-Y. Cheng, Journal of Membrane Science 369 (2011) 88–95.
[29] J. Yan, C. Liu, Z. Wang, W. Xing, M. Ding, Polymer 48 (2007) 6210–6214.
[30] O. Savard, T.J. Peckham, Y. Yang, S. Holdcroft, Polymer 49 (2008) 4949–4959.
[31] K. Chen, X. Chen, K. Yaguchi, N. Endo, M. Higa, K.-i. Okamoto, Polymer 50 (2009) 510–518.
[32] H. Pan, X. Zhu, X. Jian, Electrochimica Acta 55 (2010) 709–714.
[33] L. Wang, B.L. Yi, H.M. Zhang, D.M. Xing, The Journal of Physical Chemistry B 112 (2008) 4270–4275.
[34] X. Zhang, S. Chen, J. Liu, Z. Hu, S. Chen, L. Wang, Journal of Membrane Science 371 (2011) 276–285.
[35] S. Chen, X. Zhang, K. Chen, N. Endo, M. Higa, K.-i. Okamoto, L. Wang, Journal of Power Sources 196 (2011) 9946–9954.
[36] K. Yaguchi, K. Chen, N. Endo, M. Higa, K.-i. Okamoto, Journal of Power Sources 195 (2010) 4676–4684.
[37] S. Sundar, W. Jang, C. Lee, Y. Shul, H. Han, Journal of Polymer Science Part B: Polymer Physics 43 (2005) 2370–2379.
[38] C.-H. Lee, J.-R. Chen, H.-W. Shiu, K.-S. Ho, S.-D. Wu, K.-H. Hsieh, Y.-Z. Wang, Journal of Fuel Cell Science and Technology 7 (2010) 021023–021026.
[39] P. Zheng, T.J. McCarthy, Langmuir 26 (2010) 18585–18590.
[40] M. Okaniwa, Y. Ohta, Journal of Polymer Science Part A: Polymer Chemistry 35 (1997) 2607–2617.
[41] C.-C. Lin, W.-F. Lien, Y.-Z. Wang, H.-W. Shiu, C.-H. Lee, Journal of Power Sources 200 (2012) 1–7.
[42] L. Zou, M. Anthamatten, Journal of Polymer Science Part A: Polymer Chemistry 45 (2007) 3747–3758.
[43] C.-Y. Tseng, Y.-S. Ye, J. Joseph, K.-Y. Kao, J. Rick, S.-L. Huang, B.-J. Hwang, Journal of Power Sources 196 (2011) 3470–3478.
[44] E.A. Mistri, A.K. Mohanty, S. Banerjee, Journal of Membrane Science 411–412 (2012) 117–129.
[45] Z. Hu, Y. Yin, K. Yaguchi, N. Endo, M. Higa, K.-i. Okamoto, Polymer 50 (2009) 2933–2943.
[46] C. Genies, R. Mercier, B. Sillion, R. Petiaud, N. Cornet, G. Gebel, M. Pineri, Polymer 42 (2001) 5097–5105.
[47] C. Koning, A. Delmotte, P. Larno, B. Van Mele, Polymer 39 (1998) 3697–3702.
[48] M. Okaniwa, Y. Ohta, Journal of Polymer Science Part A: Polymer Chemistry 35 (1997) 2607–2617.
[49] X. Ye, H. Bai, W.S.W. Ho, Journal of Membrane Science 279 (2006) 570–577.
[50] C.-Y. Tseng, Y.-S. Ye, M.-Y. Cheng, K.-Y. Kao, W.-C. Shen, J. Rick, J.-C. Chen, B.-J. Hwang, Advanced Energy Materials 1 (2011) 1220–1224.
[51] J. Wang, C. Zhao, M. Li, L. Zhang, J. Ni, W. Ma, H. Na, International Journal of Hydrogen Energy.